Dalton Transactions

Accepted Manuscript

ROYAL SOCIETY OF CHEMISTRY

www.rsc.org/dalton

Cite this: DOI: 10.1039/c0xx00000x

www.rsc.org/xxxxxx

ARTICLE TYPE

Color Tunable and Near White-light Emission of Two Solvent-induced 2D Lead(II) Coordination Networks Based on Rigid Ligand 1-Tetrazole-4-imidazole-benzene

Jun Chen,[a,b] Qing Zhang,[a,b] Zhi-Fa Liu,[a] Shuai-Hua Wang,[a] Yu Xiao,[a,b] Rong Li,[a,b] Jian-Gang Xu,[a,b] Ya-Ping Zhao,[a,b] Fa-Kun Zheng,*[a] and Guo-Cong Guo*[a]

Received (in XXX, XXX) Xth XXXXXXXXX 20XX, Accepted Xth XXXXXXXXX 20XX
DOI: 10.1039/b000000x

Two new lead(II) coordination polymers, $[Pb(NO_3)(tzib)]_n$ (**1**) and $[Pb(tzib)_2]_n$ (**2**), were successfully synthesized from the reaction of rigid ligand 1-tetrazole-4-imidazole-benzene (Htzib) and lead(II) nitrate in different solvents. The obtained polymers have been characterized by single-crystal X-ray diffraction analyses, which show that both polymers feature 2D layer structures. The inorganic anion nitrate in **1** shows a μ_2-κO3:κO3 bridging mode to connect adjacent lead ions into a *zigzag* chain, and then the organic ligands $tzib^-$ join neighbored chains into a 2D layer by a μ_3-κN1:κN2:κN6 connection mode. In **2**, there are two different bridging modes of $tzib^-$ ligand: μ_3-κN1:κN2:κN6 and μ_3-κN1:κN6 to coordinate the lead ions into a 2D layer structure. Interestingly, both polymers display broadband emissions covering the entire visible spectra, which could be tunable to near white-light emission by varying excitation wavelengths.

Introduction

The exploration of white-light emitting materials and devices has drawn significant interests in recent years, because of their wide applications in lighting and displays.[1-4] Traditional approaches adopted to produce white light include exciting multiphosphors (e.g., mixing with three primary colors: red, green and blue or blue and yellow) by a UV LED,[5, 6] mixing a blue LED with a yellow phosphor,[7-9] or blending multi-LEDs, which may cause problems such as color aging or complication for device fabrication[10-12]. Direct white-light emission from a single-component entity may be expected to avoid the drawbacks of combined emitters. Therefore, the search for new single-component materials that can directly emit white light is clearly of interest and importance. To date, examples of single-component white-light emission materials are rare, but still can be found in the research field of organic molecules[13, 14] or polymers[15, 16], glass ceramics[17], metal-doped or hybrid inorganic materials[18-21], and nanomaterials[22, 23].

The luminescent coordination polymers (L-CPs), as a new type of promising light emissive materials, offer rich opportunities for developing single-component white light emitters.[24-26] Apart from metal centers[27-29] and organic linkers[30] that can produce luminescent emissive sources, metal–ligand/ligand–metal charge transfer (MLCT/LMCT)[31-33] and guest solvent molecules[34] can also generate luminescence. These luminescent emitting sources can potentially all be modulated in their relative intensities and wavelength positions, in order for the overall emission to attain the white-light quality. Generally, white-light emissions of L-CPs can be realized by following methods: (i) appropriately incorporating various lanthanide ions based on primary colors of red–green–blue (RGB) in the 4f and 3d–4f metal-L-CPs arising from lanthanide-centered emissions,[35-39] (ii) introducing different organic chromophores in one structure of Zn^{2+}/Mg^{2+}-L-CPs,[40-42] (iii) constructing Ag^+-L-CPs based on the MLCT mechanism[43] or (iv) changing the guest molecules of L-CPs[44, 45].

Currently, most of the research on L-CPs has been focused on the lanthanide metal-L-CPs[46-48] and d-block transition metal-L-CPs[49-51]. However, p-block main group metal-L-CPs have been relatively less explored. Lead(II), as a heavy p-block metal ion, owns large radius and tends to display flexible coordination behaviors, which provides unique opportunities for the formation of novel network structures.[52-55] In addition, the stereochemically active lone pairs (ns^2np^0 electron configuration) of Pb^{2+} often give rise to substantial photoluminescent processes in the Pb(II)-L-CPs involving ligand-centered transitions (e.g., $\pi^*\rightarrow$n, $\pi^*\rightarrow\pi$), ligand-to-metal charge transfer (LMCT), and metal-centered transitions.[56-58] Thus, interesting photoluminescence properties could be observed in Pb(II)-L-CPs.[56-61]

Herein, we employed 1-tetrazole-4-imidazole-benzene (Htzib) as organic ligand in the preparation of Pb-CPs, mainly based on the considerations as follows: (i) Htzib has multidentate N-coordination sites, and could display versatile coordination modes to construct CPs with fascinating structures; (ii) the rigidity of Htzib can effectively prevent non-radiative deactivation pathways, so the Htzib-based CPs may show intense photoluminescence.[62-64] In this paper, two solvent-induced Pb(II)-$tzib^-$ CPs, $[Pb(NO_3)(tzib)]_n$ (**1**) and $[Pb(tzib)_2]_n$ (**2**), have been successfully synthesized under different solvents conditions (Scheme 1).

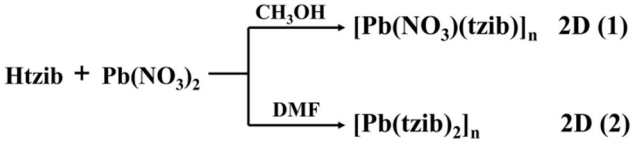

Scheme 1 The synthetic route of Pb-tzib$^-$ coordination polymers.

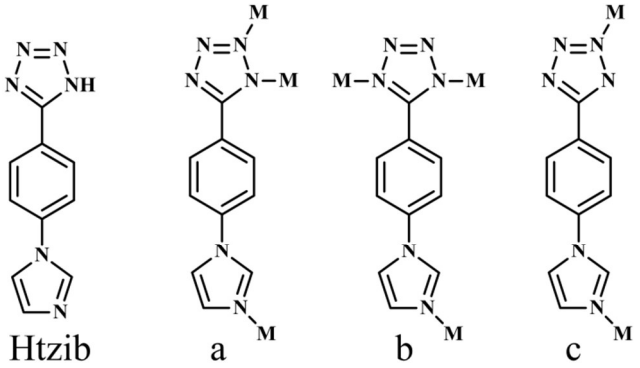

Scheme 2 The structural diagram of Htzib and three coordination modes of tzib$^-$ in compounds **1** and **2** with mode a observed in **1**, b and c in **2**.

Flexible coordination fashions of tzib$^-$ have been found in **1** and **2** (Scheme 2). Moreover, compounds **1** and **2** exhibit broadband emissions across the entire visible spectra from 400 to 700 nm, which could be tunable to direct near white-light emission by simply variation of excitation light. To the best of our knowledge, there are only few examples of Pb-CPs directly giving out white-light emissions.[65–67]

Experimental Section

Materials and Instruments

All chemicals were commercially available sources of analytical grade and used without further purification. The elemental analyses of C, H and N were determined with a Vario EL III elemental analyzer. The FT-IR spectra were recorded in the 4000–400 cm^{-1} range with a Perkin–Elmer Spectrum One Spectrometer using KBr pellets. The UV/Vis spectra were measured at room temperature using a Perkin-Elmer Lambda 900 UV–vis spectrophotometer equipped with an integrating sphere attachment and $BaSO_4$ as reference. The photoluminescence (PL) and lifetime determination were conducted on a single-grating Edinburgh EI920 fluorescence spectrometer equipped with a 450 W Xe lamp, a nF900 lamp and a PMT detector. Thermogravimetric analysis (TGA) experiments were done on a NETZSCH STA 449C Jupiter thermogravimetric analyzer in flowing nitrogen with the sample heated in an Al_2O_3 crucible at a heating rate of 5 Kmin^{-1}. All powdered X-ray diffraction data were collected on a Rigaku Miniflex II diffractometer using Cu-Kα radiation (λ = 1.540598 Å) at 40 kV and 40 mA in the range $5.00° \le 2\theta \le 65.00°$.

Syntheses of 1 and 2

[Pb(NO$_3$)(tzib)]$_n$ (1). A mixture of Htzib (0.3 mmol, 0.064 g) and $Pb(NO_3)_2$ (0.4 mmol, 0.132 g) in a methanol solvent (6 mL) was sealed into a 25mL poly(tetrafluoroethylene)-lined stainless steel container under autogenous pressure and then heated at 130 °C for 3 days and cooled to 30 °C at a rate of 2.5 °C/h. Yellow needlelike crystals suitable for X-ray analyses were obtained, washed with diethyl ether and dried in air. Yield: 76% (based on Htzib) for **1**. Anal. Calcd for $C_{10}H_7N_7O_3Pb$: C, 25.00; H, 1.47; N, 20.41%. Found: C, 24.23; H, 1.49; N, 19.84%. IR (KBr pellet, cm^{-1}): 3431 w br, 3121 m, 1614 m, 1543 s, 1508 s, 1421 s, 1385 s, 1294 s, 1196 w, 1119 m, 1069 m, 1036 m, 1005 w, 961 m, 928 m, 840 s, 760 s, 646 m, 534 m, 489 m, 428 w.

[Pb(tzib)$_2$]$_n$ (2). The procedure was the same as that for **1** except that the solvent was replaced by N,N-dimethylformamide (DMF, 4 mL). Pale yellow prismatic crystals of **2** suitable for X-ray analyses were obtained, washed with diethyl ether and dried in air. Yield: 52% (based on Htzib) for **2**. Anal. Calcd for $C_{20}H_{14}N_{12}Pb$: C, 38.15; H, 2.24; N, 26.70%. Found: C, 37.88; H, 2.32; N, 26.29%. IR (KBr pellet, cm^{-1}): 3412 m br, 3121 s, 1649 w, 1616 m, 1537 s, 1503 s, 1447 s, 1358 m, 1302 s, 1261 w, 1196 w, 1109 m, 1063 s, 1030 w, 1007 m, 962 m, 920 m, 835 m, 810 w, 764 m, 743 m, 650 m, 621 w, 538 w, 488 m, 432 w.

Single crystal structure determination

Single crystals of **1** and **2** suitable for X-ray analyses were sticked to a fiberglass. Data collections were performed on a Rigaku Saturn-70 CCD diffractometer at 293 K, which were equipped with graphite-monochromated Mo-Kα radiation (λ = 0.71073 Å). The intensity data sets were collected with the ω scan technique and reduced by CrystalClear software.[68] The structures were solved by direct methods with the SHELXTL (version 5) crystallographic software package[69] and refined by full-matrix least-squares refinement on F^2. Non-hydrogen atoms were located by difference Fourier maps and subjected to anisotropic refinement. The hydrogen atoms were added according to theoretical models. Pertinent crystal data and structure refinement results for **1** and **2** are summarized in Table 1, and selected bonds lengths and angles are listed in Table S1.

Table 1 Crystallographic data and Structural Refinements for **1** and **2**

	1	**2**
Formula	$C_{10}H_7N_7O_3Pb$	$C_{20}H_{14}N_{12}Pb$
M_r (g mol^{-1})	480.42	629.62
Space group	*Pbca*	$P2_1/c$
a/Å	12.941(4)	13.1322(11)
b/Å	6.9454(18)	7.3687(4)
c/Å	26.594(7)	21.000(2)
α/°	90	90
β/°	90	106.060(5)
γ/°	90	90
V/Å^3	2390.3(11)	1952.8(3)
Z	8	4
D_c/g cm^{-3}	2.670	2.142
μ/mm^{-1}	14.142	8.679
F(000)	1776	1200
total reflns	18867	15014
unique reflns	2724	4483
R_{int}	0.0614	0.0475
GOF	0.998	1.004
R_1 [a][$I > 2\sigma(I)$]	0.0272	0.0417
wR_2 [b](all data)	0.1134	0.1276
CCDC	1049263	1049264

[a] $R_1 = \sum(F_o - F_c)/\sum F_o$; [b] $wR_2 = [\sum w(F_o^2 - F_c^2)^2/\sum w(F_o^2)^2]^{1/2}$.

Results and Discussions

Syntheses and thermal stability

Solvent, as a significant factor in the assembly of CPs, usually plays a dominant role in affecting the coordination environment of metal ions and connection style of organic ligands.[55, 70-73] In this work, solvent-induced **1** and **2** have been succesfully synthesized under solvothermal conditions with different solvents, while the other synthetic parameters were intentionally held constant. Needlelike crystals of **1** are formed from methanol, whereas prismatic crystals of **2** are produced under DMF. The solvents used in the reaction are necessary for the formation of **1** and **2** but absent in the final structures. In addition, both **1** and **2** own 2D network structures, and the coordination geometries of Pb(II) ions in them are similar. However, the linking modes of ligands are completely different in **1** and **2**. The μ_2-κO3:κO3 bridging mode of nitrate anion and μ_3-κN1:κN2:κN6 connection mode of tzib$^-$ ligand are found in **1**, while two different coordination modes: μ_3-κN1:κN2:κN6 and μ_3-κN1:κN6 of tzib$^-$ ligand exist in **2**. The thermogravimetric analyses (TGA) experiments for **1** and **2** (Fig. S1, ESI†) were performed to investigate their thermal stability. The results show that there is no obvious weight loss before 303 °C and 278 °C for **1** and **2**, respectively, which may be the consequence of no coordination or lattice solvent molecules in their frameworks. Further heating led to rapid break down presumably due to the decomposition of inorganic anion nitrate and organic ligand tzib$^-$. However, compound **1** displays a more sharply break down manner than **2**, which can be ascribed to the existence of nitrate in **1**. Powdered X-ray diffraction (PXRD) has been measured to check the purity of the bulk samples in the solid state. The PXRD patterns of **1** and **2** closely match the simulated ones generated from the results of single-crystal diffraction, indicating a pure phase of **1** and **2** (Fig. S2, ESI†).

Structural Descriptions

[Pb(NO$_3$)(tzib)]$_n$ (1). X-ray crystallographic analysis shows that **1** crystallizes in the orthorhombic space group *Pbca* and features a 2D layer structure. There is one Pb(II) center, one inorganic anion nitrate, and one organic ligand tzib$^-$ in each asymmetric unit of **1**. As illustrated in Fig. 1, each Pb(II) atom is five-coordinated by three nitrogen atoms (N2, N1A, N6B) from three symmetry-related tzib$^-$ ligands and two oxygen atoms (O3, O3A) from two symmetry-related nitrate anions. The penta-coordinated Pb(II) atom displays a distorted square pyramidal geometry with τ_5 = 0.14 ($\tau_5 = |\beta - \alpha| / 60$, where α and β are the two biggest bond angles around the Pb(II) center; τ_5 = 0 for an ideal square pyramid, and τ_5 = 1 for an ideal trigonal bipyramid).[74] The N1A, N6B, O3 and O3A atoms constitute the equatorial plane, and N2 occupies the apical position. The bond angles around the Pb(II) atom are in the range of 69.36(19)–154.50(18)°. Both Pb–N [2.440(5)–2.667(6) Å] and Pb–O [2.522(5)–2.661(6) Å] distances are well-matched to those reported in similar coordination polymers.[55, 56, 75] Each tzib$^-$ ligand is coordinated to three Pb(II) ions through tetrazolate nitrogen (N1 and N2) and imidazole nitrogen (N6), which can be regarded as a triply bridging ligand. The O3 atom of nitrate ion represents a μ_2-bridged mode to link the adjacent Pb(II) ions into an infinite 1-D *zigzag* chain with a Pb(II)···Pb(II) shortest distance of 4.5485(10) Å (Fig. 2a). Then, the ligand tizb$^-$ joins each neighbouring chains into a 2D layer paralleled to the *ab* plane via a μ_3-κN1:κN2:κN6 connection mode (Fig. 2b). The 2D layers are tightly stacked in an –ABCD–ABCD– sequence along the *c*-direction with Van der Waals' force (Fig. 2c, Fig. S3). Moreover, no solvent molecules could be found in the unit cell of **1** calculated by PLATON software[76], which was also confirmed by TGA and elemental analysis.

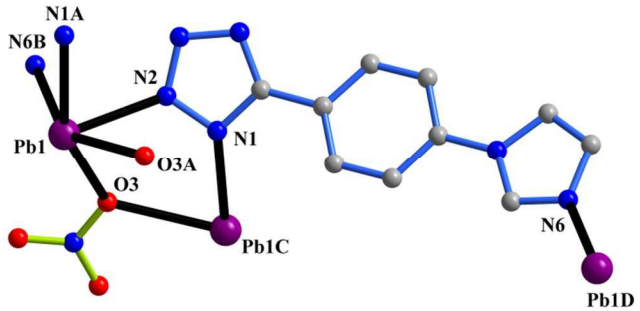

Fig. 1 The coordination environment around the Pb(II) atom and coordination mode of tzib$^-$ ligand in **1**. Symmetry codes: A: 0.5 – x, 0.5 + y, z; B: –1 + x, y, z; C: 0.5 – x, –0.5 + y, z; D: 1 + x, y, z. Hydrogen atoms are omitted for clarity.

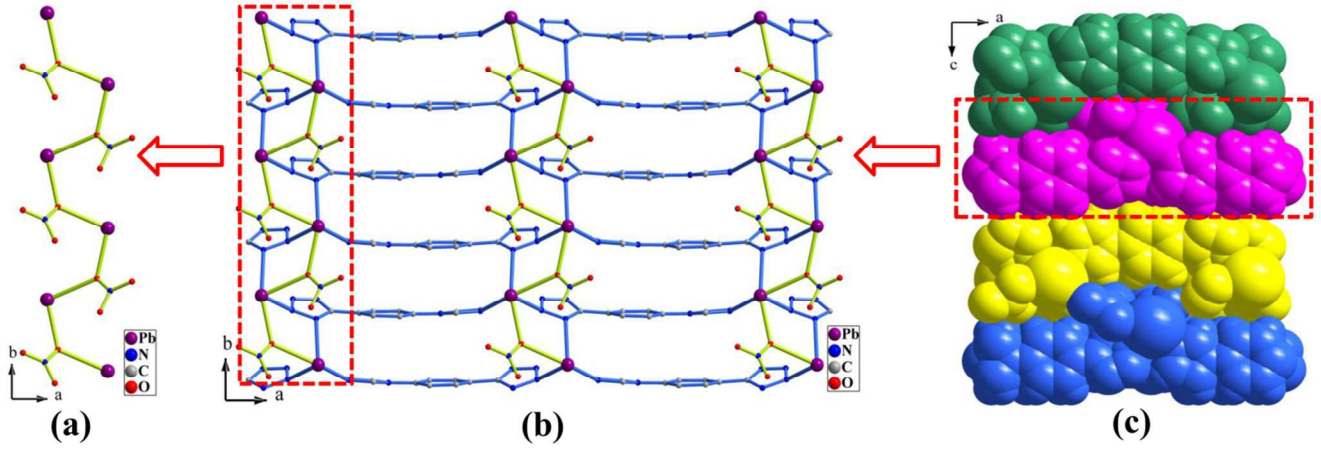

Fig. 2 (a) The 1D *zigzag* chain in **1** viewed along the *b* axis. (b) 2D network structure of **1** parallel to the *ab* plane. (c) The 2D layers stack over each other in an–ABCD–ABCD– sequence along the *c*-direction with Van der Waals' force. Hydrogen atoms are omitted for clarity.

Cite this: DOI: 10.1039/c0xx00000x

www.rsc.org/xxxxxx

ARTICLE TYPE

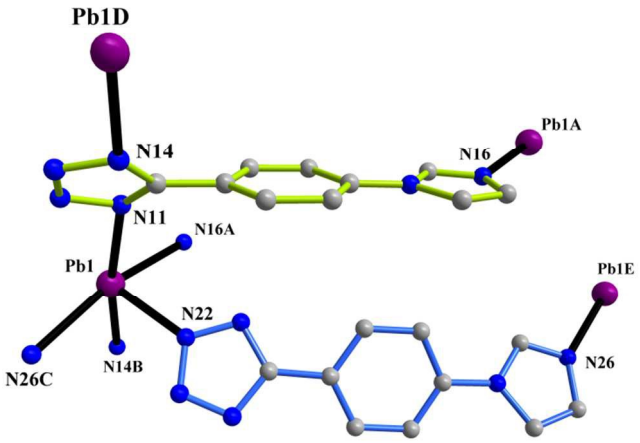

Fig. 3 The coordination environment around the Pb(II) atom and coordination mode of tzib⁻ ligand in **2**. Symmetry codes: A: 1 – x, 1 – y, – z; B: x, –1 + y, z; C: –1 + x, y, z; D: x, 1 + y, z; E: 1 + x, y, z. Hydrogen atoms are omitted for clarity.

$[Pb(tzib)_2]_n$ (2). When the reaction medium was substituted by DMF, compound **2** with a 2D layer structure was produced, which crystallizes in the monoclinic space group $P2_1/c$. Each asymmetric unit of **2** consists of one Pb(II) center, and two crystallographically independent tzib⁻ ligands (labelled as L_I and L_{II}) (Fig. 3). The L_I ligand exhibits a μ_3-κN11:κN14:κN16 coordination mode (mode b in Scheme 2), and the L_{II} ligand shows a μ_2-κN22:κN26 coordination style (mode c in Scheme 2). The Pb(II) atom is five coordinated by three N atoms from three symmetry-related L_I ligands and another two N atoms from two symmetry-related L_{II} ligands to furnish an approximately ideal square pyramidal geometry (τ_5 = 0.06) with the N–Pb–N angles varying from 79.55(19) to 171.5(2)°. The N11, N16A, N14B and N26C atoms are located at the equatorial plane, and N22 occupies the apical position. The bond lengths of Pb–N are in the normal range of 2.439(6)–2.732(7) Å and comparable to those in **1**. Each L_I ligand is coordinated to three Pb(II) ions through tetrazolate nitrogen (N11 and N14) and imidazole nitrogen (N16), which can be regarded as a triply bridging ligand. As depicted in Fig. 4a, a 1D ladder-like chain along the *b*-axis is constructed by the L_I ligand connecting the Pb(II) centers with a Pb(II)···Pb(II) shortest distance of 7.3687(5) Å. The L_{II} ligand, displaying a μ_2-bridging mode with the tetrazolate nitrogen (N22) and imidazole nitrogen (N26), further links the adjacent chains into a 2D layer (Fig. 4b, Fig. S4), which is stacked in an –AB–AB– sequence along the *c* direction (Fig. 4c). The π-stacking interactions exist between adjacent layers, which would be better described as C–H···π attractions, with a ca. 2.660 Å distance of H26 to the neighboring tetrazolate ring (Fig. 4d). Similar with **1**, there is not any solvent molecule in the unit cell of **2** calculated by PLATON software,[76] and further confirmed by TGA and elemental analysis.

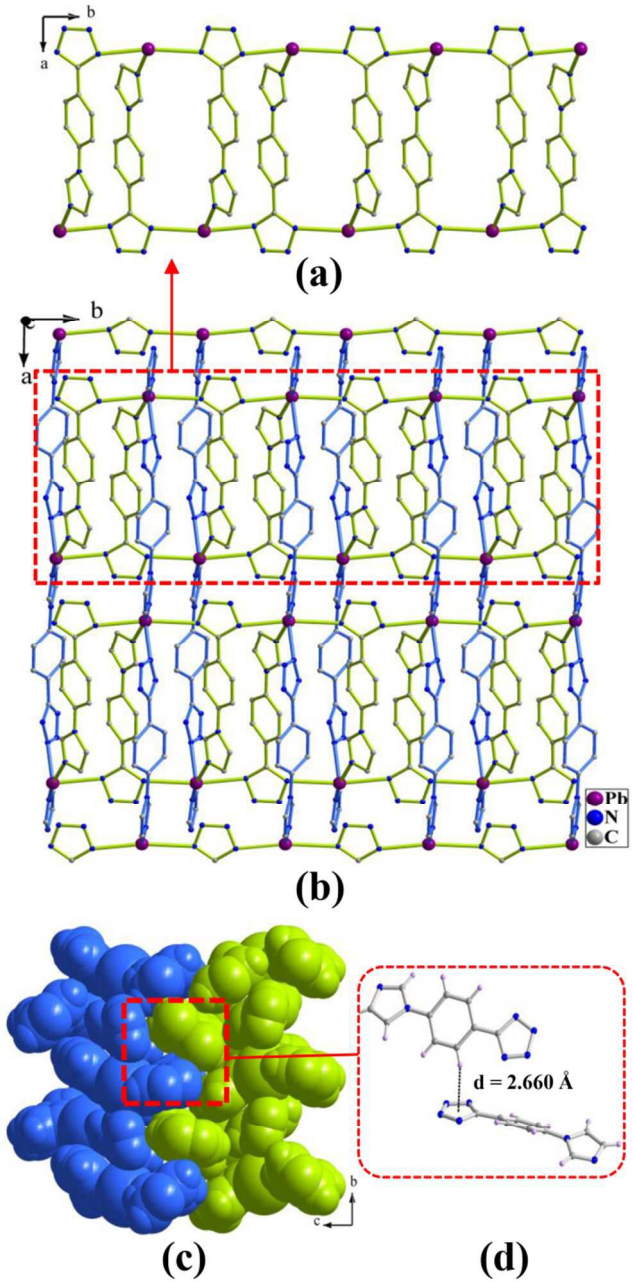

Fig. 4 (a) A 1D ladder-like chain of **2** viewed along the *b*-axis. (b) 2D layer structure of **2** parallel to the *ab* plane. (c) –AB–AB– layered arrangement of **2** along the *c* axis. (d) C–H···π interactions between the two adjacent layers.

Optical properties for 1 and 2

The solid-state UV/Vis spectras of **1** and **2**, as well as the free ligand Htzib, display intense absorption bands in the UV range (Fig. S5, ESI†), which can be mainly assigned to the π–π^* charge transfer. As a rigid organic ligand, Htzib exhibits intense blue emission when excited by UV-light. Upon changing excitation

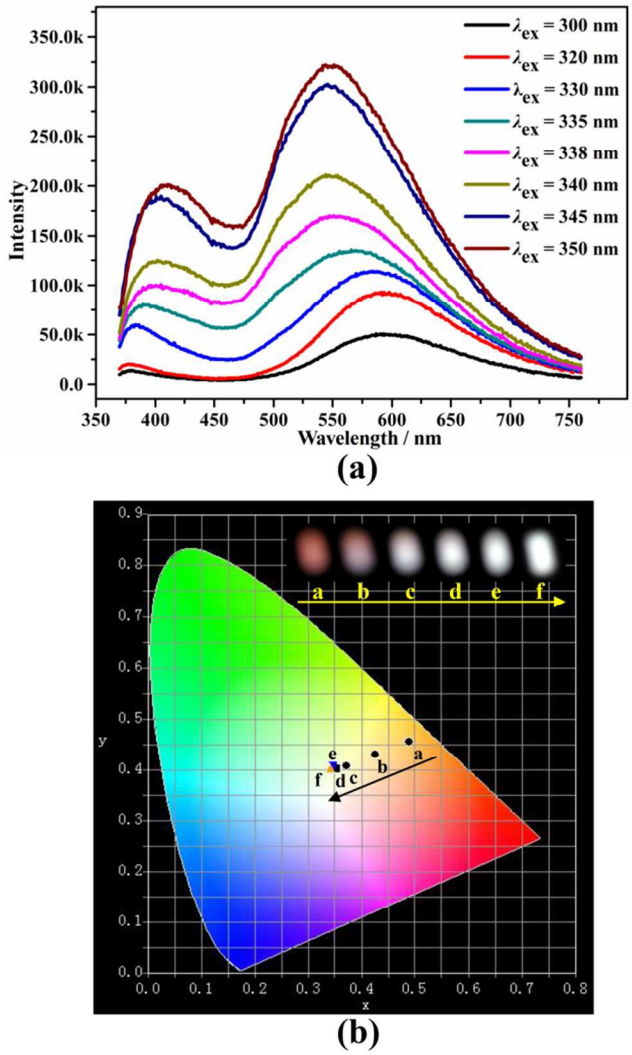

Fig. 5 (a) Solid-state photoluminescent spectra of **1** by varying excitation wavelengths. (b) The photograph of the CIE chromaticity diagrams for **1**; the inset is the photoluminescent images of **1** excited by 320, 330, 335, 338, 340 and 350 nm light, respectively.

wavelengths from 300 to 350 nm, Htzib shows a maximum emission at ~380 nm (Fig. S6, ESI†), and the overall emission is always in the blue region, as illustrated by the CIE (CIE = Commission International de l'Echairage) chromaticity coordinates of the emission spectra in Fig. S7 (ESI†). Such emissions observed in the free ligand Htzib can be assigned to the typical ligand-centered transitions. Interestingly, both lead(II) polymers **1** and **2** display broadband emissions across the entire visible spectra from 400 to 700 nm, which could be tunable to direct near white-light emission by simply variation of excitation light. Their solid-state luminescence has been investigated at room temperature.

As depicted in Fig. 5a, polymer **1** features a dominant emission band at ~595 nm, and a relative weak band at ~380 nm when excited by 300–320 nm light. With increase of the excitation wavelengths from 320 to 340 nm, the lower-energy (LE) emission band is enhanced, and displays an obvious blue shift from ~595 to ~546 nm. Meanwhile, the higher-energy (HE) emission band is enhanced more rapidly than the LE band, and exhibits a little red shift from ~380 to ~402 nm. As a result, the overall emissions gradually evolve from orange to near white-light by changing excitation wavelengths, and its corresponding CIE chromaticity coordinates exhibit an easy intuitive change (Fig. 5b, Table S2). Further increase of the excitation wavelengths from 340 to 350 nm mainly affects the intensity of photoluminescence, and the HE emission band displays a little red shift from ~402 to ~410 nm. However, the overall emission is always located in the near white-light region. When excited by 338 nm light, the optimized CIE chromaticity coordinate of (0.35, 0.40), color-rendering index (CRI) of 80 and correlated color temperature (CCT) of 4909 K, result in a "warm" white-light sought for many indoor lighting applications.

The solid-state sample of **2** dislays two obvious emission bands with maxima at ~385 and ~525 nm upon excitation in the range of 320–350 nm, which are located in the blue and yellow-greenish light region, respectively. The relative intensity of the emission bands can be tunable upon changing excitation wavelengths. As shown in Fig. 6a, with the exictation wavelength increased, both the blue HE emission band and yellow-greenish LE emission band are enhanced, but the HE one is strengthened more quickly than the LE one. When the excitation wavelengths further rise from 360 to 385 nm, the HE emission band exhibits a red shif to 438–465 nm, while the intensity of LE emission band is gradully weakened (Fig. 6b). From the CIE chromaticity diagram (Fig. 6c, Table S3), it is clear that the

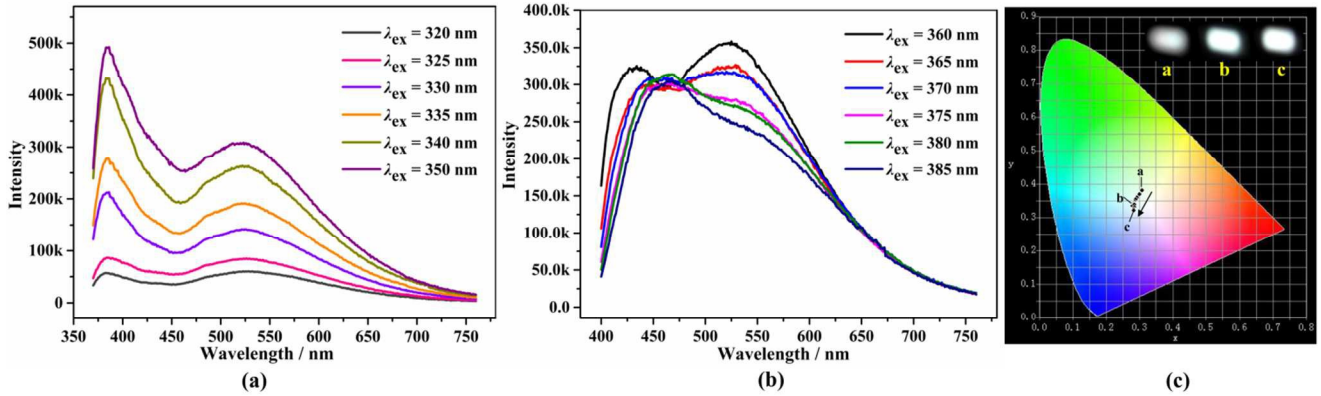

Fig. 6 (a) and (b) Solid-state photoluminescent spectra of **2** by varying excitation wavelengths. (c) The photograph of the CIE chromaticity diagrams for **2**; the inset represents the photoluminescent images of **2** excited by 320, 350 and 385 nm light, respectively.

Cite this: DOI: 10.1039/c0xx00000x

www.rsc.org/xxxxxx

ARTICLE TYPE

photoluminescences of **2** are all located in the white-light region throughout the excitation wavelengths ranging from 320 to 385 nm. Such remarkable persistence of the white light feature observed in **2** is rare, and provides advantages for lighting applications. The chromaticity coordinate for **2** is (0.29, 0.33) when irradiated by 375 nm light, which is closer to the pure white-light (0.33, 0.33) than the reported white-light emitting Pb(II)-CP (0.27, 0.30).[66] In addition, the CRI of 84 and CCT of 8166 K are also monitored at 375 nm, which affords a "cold" white light. Moreover, the emission decay times of **1** and **2** have been detected at room temperature. The 380 nm (λ_{ex} = 320 nm), 595 nm (λ_{ex} = 320 nm), 402 nm (λ_{ex} = 340 nm) and 546 nm (λ_{ex} = 340 nm) peaks of **1** have lifetimes of 2.4 ns, 2.7 ns, 2.4 ns and 2.6 ns, respectively (Fig. S8, ESI†), while the 384 nm (λ_{ex} = 350 nm) and 525 nm (λ_{ex} = 350 nm) peaks of **2** have lifetimes of 3.2 ns and 4.1 ns, respectively (Fig. S9, ESI†), which indicates that they both have fluorescence characteristics.

The emitting behaviour of **1** and **2** can be regarded as a dual-emissive resource, and the two emission bands in them arise from different origins. The LE bands beyond 520 nm are significantly red-shifted compared to that of the free ligand, which can be attributed to ligand-to-metal charge transfer between the π systems and the p orbitals of the Pb^{2+} centers.[33, 60, 65, 66] It needs to note that the variations of LE bands in **1** and **2** are totally different upon changing excitation wavelengths. In **1**, with the increase of the excitation wavelengths from 320 to 350 nm, the LE emission band is enhanced, and displays a gradual blue shift from ~595 to ~546 nm. While in **2**, the excitation variations mainly affect the relative intensity of the LE emission bands. Such differences mainly stem from different components and structures of **1** and **2**. Polymer **1** simultaneously contains organic $tzib^-$ ligand and inorganic anion nitrate. Apart from the $tzib^-$, the inorganic nitrate anion also owns π electrons, which may have contribution to the LMCT. However, polymer **2** only contains organic $tzib^-$ ligand, and the π electrons only come from the aromatic rings of $tzib^-$. Therefore, the different π systems in **1** and **2** might be the essential reason for different variation behaviours of LE bands in **1** and **2**. On the other hand, the HE bands centering at 380–465 nm in the emission spectra of **1** and **2** can be assigned to π–π* charge transfer. Similar with the variation trend of LE bands, the nitrate anion also has effects on the HE bands of **1**. With the excitation lengths varying from 320 to 350 nm, the HE emission bands of **1** show a gradual red shift from ~380 to ~410 nm. As to **2**, the intensity of the HE emission bands varies upon changing the excitation wavelengths from 320 to 350 nm, which is similar with the emissive property of the free ligand Htzib. The excitation spectra **1** and **2** monitored at two maximum emissions are demonstrated in Figs. S10 and S11, ESI†).

Conclusion

In summary, we have successfully obtained two solvent-induced lead(II) coordination polymers by solvothermal synthesis of rigid ligand 1-tetrazole-4-imidazole-benzene and lead(II) nitrate in different solvents conditions. Both **1** and **2** feature 2D layer structures with the lead(II) center in a penta-coordinated environment. The structural differences between them mainly arise from the different connection modes of the organic ligand $tzib^-$, which can be affected by the reaction solvents. Luminescence investigation indicates that polymers **1** and **2** display dual-emissive behaviors, and their photoluminescence is tunable. Direct white-light emissions could be achieved upon simply varying excitation wavelengths. Therefore, polymers **1** and **2**, as single-component white-light emitting materials, could be potential application in white-light devices fabrication. We believe that more single-component white-light Pb-CPs with better luminescence quality might be obtained through replacement of Htzib by other rigid ligands.

Acknowledgements

This work was financially supported by 973 Program (2011CBA00505) and National Nature Science Foundation of China (21371170).

Notes and references

[a] *State Key Laboratory of Structural Chemistry, Fujian Institute of Research on the Structure of Matter, Chinese Academy of Sciences, Fuzhou, Fujian 350002, P. R. China. Fax: (+86) 591-8371-4946; Tel:86-591-83704827; E-mail: zfk@fjirsm.ac.cn;*

[b] *University of Chinese Academy of Sciences, Beijing 100039, P. R. China.*

† Electronic Supplementary Information (ESI) available: X-ray crystallographic files in CIF format of **1** and **2**, selected bond lengths and angles, thermochemical properties, PXRD patterns, solid-state UV/Vis absorbance spectra, photoluminescent spectra and CIE chromaticity diagram for Htzib, photoluminescence lifetime data and fitted curves, and FT-IR spectra. See DOI: 10.1039/b000000x/.

1. P. Waltereit, O. Brandt, A. Trampert, H. T. Grahn, J. Menniger, M. Ramsteiner, M. Reiche and K. H. Ploog, *Nature*, 2000, **406**, 865–868.
2. E. Jang, S. Jun, H. Jang, J. Llim, B. Kim and Y. Kim, *Adv. Mater.*, 2010, **22**, 3076–3080.
3. J. S. Kim, P. E. Jeon, Y. H. Park, J. C. Choi, H. L. Park, G. C. Kim and T. W. Kim, *Appl. Phys. Lett.*, 2004, **85**, 3696–3698.
4. G. Li, T. Fleetham and J. Li, *Adv. Mater.*, 2014, **26**, 2931–2936.
5. X. Gong, S. Wang, D. Moses, G. C. Bazan and A. J. Heeger, *Adv. Mater.*, 2005, **17**, 2053–2058.
6. J. Kido, M. Kimura and K. Nagai, *Science*, 1995, **267**, 1332–1334.
7. C. Zhao, D. C. Zhu, W. Gao, M. J. Tu, L. L. Luo, T. Han and X. L. Jing, *Chem. Eng. J.*, 2014, **254**, 486–490.
8. X. F. Li, J. D. Budai, F. Liu, J. Y. Howe, J. H. Zhang, X. J. Wang, Z. J. Gu, C. J. Sun, R. S. Meltzer and Z. W. Pan, *Light-Science & Applications*, 2013, **2**, e50.
9. C. Fan and C. Yang, *Chem. Soc. Rev.*, 2014, **43**, 6439–6469.
10. G. L. Tu, C. Y. Mei, Q. G. Zhou, Y. X. Cheng, Y. H. Geng, L. X. Wang, D. G. Ma, X. B. Jing and F. S. Wang, *Adv. Funct. Mater.*, 2006, **16**, 101–106.
11. B. P. Yan, C. C. C. Cheung, S. C. F. Kui, H. F. Xiang, V. A. L. Roy, S. J. Xu and C. M. Che, *Adv. Mater.*, 2007, **19**, 3599–3603.
12. B. W. D'Andrade, R. J. Holmes and S. R. Forrest, *Adv. Mater.*, 2004, **16**, 624–628.

13. X. H. Jin, C. Chen, C. X. Ren, L. X. Cai and J. Zhang, *Chem. Commun.*, 2014, **50**, 15878–15881.
14. Q. Y. Yang and J. M. Lehn, *Angew. Chem. Int. Ed. Engl.*, 2014, **53**, 4572–4577.
15. H. B. Wu, G. J. Zhou, J. H. Zou, C. L. Ho, W. Y. Wong, W. Yang, J. B. Peng and Y. Cao, *Adv. Mater.*, 2009, **21**, 4181–4184.
16. H. B. Wu, L. Ying, W. Yang and Y. Cao, *Chem. Soc. Rev.*, 2009, **38**, 3391–3400.
17. R. Zhang, H. Lin, Y. L. Yu, D. Q. Chen, J. Xu, Y. S. Wang, *Laser & Photonics Rev.*, 2014, **8**, 158–164.
18. S. K. Panda, S. G. Hickey, H. V. Demir and A. Eychmuller, *Angew. Chem. Int. Ed.*, 2011, **50**, 4432–4436.
19. Z. G. Xia, J. Q. Zhuang and L. B. Liao, *Inorg. Chem.*, 2012, **51**, 7202–7209.
20. E. R. Dohner, E. T. Hoke and H. I. Karunadasa, *J. Am. Chem. Soc.*, 2014, **136**, 1718–1721.
21. E. R. Dohner, A. Jaffe, L. R. Bradshaw and H. I. Karunadasa, *J. Am. Chem. Soc.*, 2014, **136**, 13154–13157.
22. T. E. Rosson, S. M. Claiborne, J. R. McBride, B. S. Stratton and S. J. Rosenthal, *J. Am. Chem. Soc.*, 2012, **134**, 8006–8009.
23. J. H. Kim, Y. H. Ko, J. H. Cho, S. H. Gong, S. M. Ko and Y. H. Cho, *Nanoscale*, 2014, **6**, 14213–14220.
24. J. Heine and K. Muller-Buschbaum, *Chem. Soc. Rev.*, 2013, **42**, 9232–9242.
25. Y. Liu, M. Pan, Q. Y. Yang, L. Fu, K. Li, S. C. Wei and C. Y. Su, *Chem. Mater.*, 2012, **24**, 1954–1960.
26. M. D. Allendorf, C. A. Bauer, R. K. Bhakta and R. J. T. Houk, *Chem. Soc. Rev.*, 2009, **38**, 1330–1352.
27. J. Chen, Q. Zhang, F. K. Zheng, Z. F. Liu, S. H. Wang, A. Q. Wu and G. C. Guo, *Dalton Trans*, 2015, **44**, 3289–3294.
28. Y. H. Han, C. B. Tian, Q. H. Li and S. W. Du, *J. Mater. Chem. C*, 2014, **2**, 8065–8070.
29. K. Miyata, T. Nakagawa, R. Kawakami, Y. Kita, K. Sugimoto, T. Nakashima, T. Harada, T. Kawai and Y. Hasegawa, *Chemistry*, 2011, **17**, 521–528.
30. Z. Wei, Z. Y. Gu, R. K. Arvapally, Y. P. Chen, R. N. McDougald, Jr., J. F. Ivy, A. A. Yakovenko, D. Feng, M. A. Omary and H. C. Zhou, *J. Am. Chem. Soc.*, 2014, **136**, 8269–8276.
31. L. Z. Cai, M. S. Wang, M. J. Zhang, G. E. Wang, G. C. Guo and J. S. Huang, *CrystEngComm*, 2012, **14**, 6196–6200.
32. S. L. Zheng, J. H. Yang, X. L. Yu, X. M. Chen and W. T. Wong, *Inorg. Chem.*, 2004, **43**, 830–838.
33. Y. H. Zhao, H. B. Xu, Y. M. Fu, K. Z. Shao, S. Y. Yang, Z. M. Su, X. R. Hao, D. X. Zhu and E. B. Wang, *Cryst. Growth Des.*, 2008, **8**, 3566–3576.
34. N. B. Shustova, B. D. McCarthy and M. Dinca, *J. Am. Chem. Soc.*, 2011, **133**, 20126–20129.
35. Z. F. Liu, M. F. Wu, S. H. Wang, F. K. Zheng, G. E. Wang, J. Chen, Y. Xiao, A. Q. Wu, G. C. Guo and J. S. Huang, *J. Mater. Chem. C*, 2013, **1**, 4634–4639.
36. H. B. Zhang, X. C. Shan, L. J. Zhou, P. Lin, R. F. Li, E. Ma, X. G. Guo and S. W. Du, *J. Mater. Chem. C*, 2013, **1**, 888–891.
37. D. F. Sava, L. E. Rohwer, M. A. Rodriguez and T. M. Nenoff, *J. Am. Chem. Soc.*, 2012, **134**, 3983–3986.
38. Y. Wei, Q. Li, R. Sa and K. Wu, *Chem Commun*, 2014, **50**, 1820–1823.
39. Q. Y. Yang, K. Wu, J. J. Jiang, C. W. Hsu, M. Pan, J. M. Lehn and C. Y. Su, *Chem Commun*, 2014, **50**, 7702–7704.
40. S. Q. Zhang, F. L. Jiang, Y. Bu, M. Y. Wu, J. Ma, X. C. Shan, K. C. Xiong and M. C. Hong, *CrystEngComm*, 2012, **14**, 6394–6396.
41. Y. Q. Wei, K. C. Wu, J. G. He, W. X. Zheng and X. Y. Xiao, *CrystEngComm*, 2011, **13**, 52–54.
42. Z. F. Wu, B. Tan, J. Y. Wang, C. F. Du, Z. H. Deng and X. Y. Huang, *Chem Commun*, 2015, **51**, 157–160.
43. M. S. Wang, S. P. Guo, Y. Li, L. Z. Cai, J. P. Zou, G. Xu, W. W. Zhou, F. K. Zheng and G. C. Guo, *J. Am. Chem. Soc.*, 2009, **131**, 13572–13573.
44. N. Yanai, K. Kitayama, Y. Hijikata, H. Sato, R. Matsuda, Y. Kubota, M. Takata, M. Mizuno, T. Uemura and S. Kitagawa, *Nature Materials*, 2011, **10**, 787–793.
45. M. J. Dong, M. Zhao, S. Ou, C. Zou and C. D. Wu, *Angew. Chem. Int. Ed. Engl.*, 2014, **53**, 1575–1579.
46. J. Rocha, L. D. Carlos, F. A. A. Paz and D. Ananias, *Chem. Soc. Rev.*, 2011, **40**, 926–940.
47. M. F. Wu, M. S. Wang, S. P. Guo, F. K. Zheng, H. F. Chen, X. M. Jiang, G. N. Liu, G. C. Guo and J. S. Huang, *Cryst. Growth Des.*, 2011, **11**, 372–381.
48. D. F. Sava Gallis, L. E. S. Rohwer, M. A. Rodriguez and T. M. Nenoff, *Chem. Mater.*, 2014, **26**, 2943–2951.
49. M. F. Wu, Z. F. Liu, S. H. Wang, J. Chen, G. Xu, F. K. Zheng, G. C. Guo and J. S. Huang, *CrystEngComm*, 2011, **13**, 6386–6392.
50. S. H. Wang, F. K. Zheng, M. J. Zhang, Z. F. Liu, J. Chen, Y. Xiao, A. Q. Wu, G. C. Guo and J. S. Huang, *Inorg. Chem.*, 2013, **52**, 10096–10104.
51. M. F. Wu, F. K. Zheng, A. Q. Wu, Y. Li, M. S. Wang, W. W. Zhou, F. Chen, G. C. Guo and J. S. Huang, *CrystEngComm*, 2010, **12**, 260–269.
52. L. Zhang, Z. J. Li, Q. P. Lin, Y. Y. Qin, J. Zhang, P. X. Yin, J. K. Cheng and Y. G. Yao, *Inorg. Chem.*, 2009, **48**, 6517–6525.
53. D. Deng, L. Liu, B.-M. Ji, G. Yin and C. Du, *Cryst. Growth Des.*, 2012, **12**, 5338–5348.
54. C. Gabriel, C. P. Raptopoulou, A. Terzis, V. Psycharis, F. Gul-E-Noor, M. Bertmer, C. Mateescu and A. Salifoglou, *Cryst. Growth Des.*, 2013, **13**, 2573–2589.
55. J. Li, G. Yang, L. Hou, L. Cui, Y. Li, Y. Y. Wang and Q. Z. Shi, *Dalton Trans*, 2013, **42**, 13590–13598.
56. J. Y. Sun, D. J. Zhang, L. Wang, Y. Cao, D. Li, L. Y. Zhang, W. Song, Y. Fan and J. N. Xu, *CrystEngComm*, 2012, **14**, 3982–3989.
57. O. Toma, N. Mercier, M. Bouilland and M. Allain, *CrystEngComm*, 2012, **14**, 7844–7847.
58. W. W. Lestari, P. Lönnecke, H. C. Streit, M. Handke, C. Wickleder and E. Hey-Hawkins, *Eur. J. Inorg. Chem.*, 2014, **2014**, 1775–1782.
59. L. N. Li, S. Q. Zhang, L. Han, Z. H. Sun, J. H. Luo and M. C. Hong, *Cryst. Growth Des.*, 2013, **13**, 106–110.
60. X. L. Wang, Y. Q. Chen, Q. Gao, H. Y. Lin, G. C. Liu, J. X. Zhang and A. X. Tian, *Cryst. Growth Des.*, 2010, **10**, 2174–2184.
61. J. Sun, D. Zhang, L. Wang, Y. Cao, D. Li, L. Zhang, W. Song, Y. Fan and J. Xu, *CrystEngComm*, 2012, **14**, 3982–3988.
62. X. Wang, J. Peng, K. Alimaje and Z. Y. Shi, *CrystEngcomm*, 2012, **14**, 8509–8514.
63. Z. Y. Shi, Z. Y. Zhang, J. Peng, X. Yu and X. Wang, *CrystEngcomm*, 2013, **15**, 7199–7205.
64. P. Du, Y. Yang, D. W. Kang, J. Yang, Y. Y. Liu and J. F. Ma, *CrystEngcomm*, 2014, **16**, 6372–6379.
65. A. C. Wibowo, S. A. Vaughn, M. D. Smith and H. C. Zur Loye, *Inorg. Chem.*, 2010, **49**, 11001–11008.
66. J. He, M. Zeller, A. D. Hunter and Z. Xu, *J. Am. Chem. Soc.*, 2012, **134**, 1553–1559.
67. M. Pan, C. Yan, L. Chen, L. Y. Zhang, S. Y. Yin, Y. X. Zhu, K. Wu, Y. J. Hou, C. Y. Su, *New J. Chem.*, 2015, DOI: 10.1039/C5NJ00168D
68. CrystalClear, version 1.35; Software User's Guide for the Rigaku R-Axis and Mercury and Jupiter CCD Automated X-ray Imaging System; Rigaku Molecular Structure Corporation: UT, 2002.
69. SHELXTL Reference Manual, version 5; Siemens Energy & Automation Inc.: Madison, WI, 1994.
70. A. Santra and P. K. Bharadwaj, *Cryst. Growth Des.*, 2014, **14**, 1476–1485.
71. P. Cui, J. Wu, X. Zhao, D. Sun, L. Zhang, J. Guo and D. Sun, *Cryst. Growth Des.*, 2011, **11**, 5182–5187.
72. L. L. Qu, Y. L. Zhu, Y. Z. Li, H. B. Du and X. Z. You, *Cryst. Growth Des.*, 2011, **11**, 2444–2452.
73. L. N. Li, S. Y. Wang, T. L. Chen, Z. H. Sun, J. H. Luo and M. C. Hong, *Cryst. Growth Des.*, 2012, **12**, 4109–4115.
74. L. Yang, D. R. Powell and R. P. Houser, *Dalton Trans*, 2007, **36**, 955–964.
75. C. Gabriel, M. Perikli, C. P. Raptopoulou, A. Terzis, V. Psycharis, C. Mateescu, T. Jakusch, T. Kiss, M. Bertmer and A. Salifoglou, *Inorg. Chem.*, 2012, **51**, 9282–9296.
76. A. L. Spek, PLATON, A Multipurpose Crystallographic Tool, Utrecht University, The Netherlands, 2005.

Table of Contents

Color Tunable and Near White-light Emission of Two Solvent-induced 2D Lead(II) Coordination Networks Based on Rigid Ligand 1-Tetrazole-4-imidazole-benzene

Jun Chen,[a,b] Qing Zhang,[a,b] Zhi-Fa Liu,[a] Shuai-Hua Wang,[a] Yu Xiao,[a,b] Rong Li,[a,b] Jian-Gang Xu,[a,b] Ya-Ping Zhao,[a,b] Fa-Kun Zheng,*[a] and Guo-Cong Guo*[a]

[a] *State Key Laboratory of Structural Chemistry, Fujian Institute of Research on the Structure of Matter, Chinese Academy of Sciences, Fuzhou, Fujian 350002, P. R. China;* [b] *University of Chinese Academy of Sciences, Beijing 100039, P. R. China*

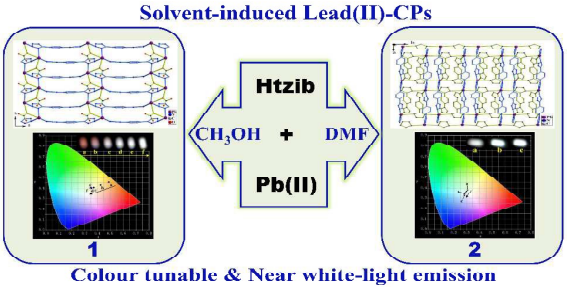

Two solvent-induced Pb(II)-tzib^{-} (Htzib = 1-tetrazole-4-imidazole-benzene) coordination polymers display color tunable and near white-light emissions upon varying excitation wavelengths.